Power Requirements of Ground-Based Bushfire Detection Devices

Timothy Alder
u7287129

October 5, 2022

Report submitted for **ENGN2706** at the School of Engineering, Australian National University

Project Supervisor: **Dr. Salman Durrani**

Abstract

Recently, there has been increased interested in the use of ground-based Internet of Things (IoT) sensors for bushfire detection applications. Such a system typically comprises sensors and a gateway to collect information and relay it to a control station. A key requirement of such systems is that devices are optimised for the lowest possible power consumption. This paper will focus on the power requirements of such a system and seek to evaluate the feasibility of various power sources. Power consumption is investigated for various detection methods. This is used to calculate lifetime power consumption for various combinations of detection methods (device configurations) under different operating conditions. Finally, research is conducted into several potential power sources. This concludes with a recommendation for a secondary cell with a solar panel for visual detection methods and a primary cell for all other detection methods.

Contents

1 Introduction

1.1 Impacts of Australian Bushfires

Beginning June of 2019, Australia experienced it's most devastating bushfire season in recorded history. Peaking in December of 2019 and January of 2020, the fires lasted until October of 2020 and are estimated to have burnt over twenty-million hectares [1]. The estimated CO2 emissions of the fires alone were nearly double Australia's average annual fossil fuel and bushfire emissions [2]. Even ignoring their calamitous environmental impact [1]-[3], the fires plunged Australian air quality to the worst in the world [4]-[5], lost billions in tourism and agricultural revenue [5]-[6], and are forecast to have a cost totalling tens of billions of dollars [3],[5]-[6].

Perhaps the most alarming story of the 2019-20 Australian bushfire season is that of the Orroral Valley bushfire in the Australian Capital Territory. The Orraral Valley bushfire began in January of 2020, burning through some 80% of Namadgi National Park (82,700 acres) and 20% of Tidbinbilla Nature Reserve (1,444 acres) [7]. Though it was one of the smaller bushfires in Australia at the time, the nature of the fires ignition was particularly distressing, having been sparked by the tail landing light of a defence helicopter [8]. The small grass fire was then fanned into a firestorm by the ascending helicopters rotor. The helicopter flew for close to an hour before alerting authorities to the fires location. Rather ironically, the helicopter was initially on a reconnaissance mission as part of Operation Bushfire Assist. In total, it took ACT emergency services 48 minutes to pinpoint the fire's location, roughly the same time at which the helicopters pilots notified emergency services to the incident.

With such devastating impacts in just a single bushfire season, the need for better, more comprehensive bushfire management strategies in Australia is obvious. Presently, the primary methods of bushfire detection are human-manned watchtowers, spotter aircraft and satellites. Of these detection methods, satellites are most comprehensive; however, unsurprisingly, they are also the most costly and face other limitations such as refresh rate and detection threshold. Comparatively, spotter aircraft and watchtowers are far cheaper, however, they are also far less comprehensive, ineffective during the night and limited by their ability to detect a fire quickly. With the advent of the Internet of Things (IoT), ground-based bushfire detection sensors present a low-cost alternative to other detection methods, and are capable of monitoring on a truly comprehensive scale. Most commonly, these detection sensors use a combination of temperature, humidity, gas, audial, optical and air pressure sensors, and are capable of achieving effective detection rates over 90% [9].

1.2 Research Question

This paper seeks to estimate the operational power consumption of various ground-based bushfire detection devices and provide a recommendation as to what power supply should be used for each of the identified detection methods.

1.3 Project Scoping

Given the short time frame of this project, it is important to define the projects assumptions and boundaries that were specified during scoping. These are outlined below.

- The project models power consumption with a minimum of three distinct, simplified operating states.
- The project does not examine every possible component combination, however, the method used and data gathered serve as a guide such that calculations may be performed for any combination of the readers choosing.
- The project does not consider the use of a prediction matrix to control the activation of certain components.
- The project does not examine every possible method of fire detection. Instead, it only considers those which have demonstrated effectiveness in a research or commercial use case.

1.4 Report Structure

The structure of the project is outlined as follows:

Literature Review
This section examines existing ground-based detection solutions to identify sensors and power sources with proven existing applications in a ground-based bushfire detection context.

Component Analysis
This section uses the literature review to compile a list of components used in the detection of fires. For each component, a brief explanation is given clarifying it's relevance to fire detection. Where applicable, an investigation is conducted into the power consumption of existing commercially available products.

Sensor Configurations
This section uses the component analysis to model the lifetime operational power consumption of specific combinations of sensors. The model is then used to estimates the total possible range of lifetime power consumption.

Potential Power Supplies
This section uses the literature review to compile a list of power supplies that could potentially be used, in a remote, IoT fire detection application.

Results
This section assigns power supplies to specific ranges of lifetime operational power consumption using an informal cost-effectiveness analysis.

Conclusion and Future Works
This section summarises the findings of the paper and provides some examples as to how future researchers might use the contents of this paper.

2 Literature Review

2.1 Existing ground-based bushfire detection sensors

In line with the paper's context, this section focuses on existing ground-based detection solutions. The purpose of this subsection is to identify sensors and power sources with proven existing applications in a ground-based bushfire detection context. Where ever

possible, the cost of an identified detection method will also be discussed. The remainder of the report will then conduct a detailed analysis of the power requirements for each identified component and recommend power sources for a number of different sensor configurations. Majority of the entities examined in this literature review are sourced from 'Firetech Connect' [10], an initiative of the Peregrin Digital Hub in Noosa.

2.1.1 Dryad

Ground-based bushfire detection sensors have been implemented at varying scales across the world. For example, German-based company, Dryad, offer an early detection system that uses gas, temperature, smoke, humidity and air pressure sensors to detect gases emitted by bushfires during the smouldering phase [11]. Dryad's Wildfire Sensors (DWS) are powered by supercapacitors and charged by a 6cm^2 solar panel, achieving a maintenance-free lifetime up to fifteen years. Each DWS is capable of monitoring a 100m radius area within which a 2m^2 fire will be detected in under an hour from ignition. DWS's are designed to be mounted on trees and are roughly 20x10cm in size.*

In typical deployment, 100 DWS form a mesh network that communicates with a Silvanet Mesh Gateway device (SMG). The SMG has an increased communication range of 2-6km [12]. Like the WDS, SMGs are powered by supercapacitors and charged by a larger solar panel (roughly 60x25cm). Both DWS and SMG's communicate using low-power, wide area networking protocol (LoRaWAN). Notably, SMGs are capable of connecting to other devices (besides WDS's) through LoRaWAN, presenting the possibility for significantly more functionality in the future.**

Multiple SMGs form a secondary mesh network that relays data to a Silvanet Border Gateway (SBG). In typical deployment, 20 SMGs are placed for each SBG. Figure 1 illustrates the network configuration between Dryad devices [11]-[13]. The SBG can be powered by either solar panel or mains power and also includes a supercapacitor for energy storage. The SBG features 4G, 2G and Ethernet connectivity or satellite up/down link for remote deployments.*** As of writing, Dryad are seeking to deliver on 10, paid proof-of-concept installations across five continents [14].

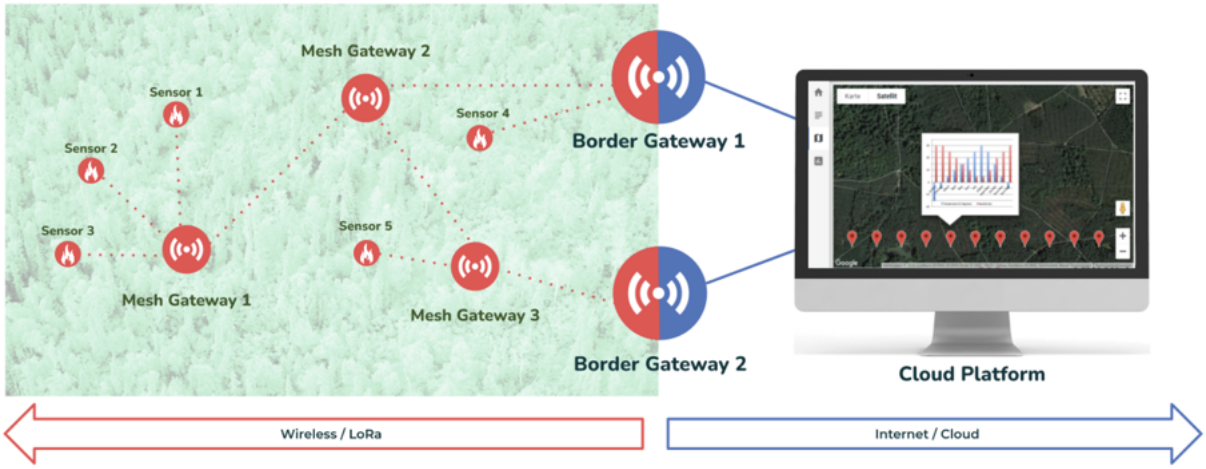

Figure 1: Network configuration of Dryad devices [11]-[13].

* A copy of the full DWS datasheet can be found in Appendix A
** A copy of the full SMG datasheet can be found in Appendix B
*** A copy of the full SBG datasheet can be found in Appendix C

2.1.2 Attentis

Australian-based company, Attentis, offer comprehensive microclimate monitoring sensors that can be customised to the users needs. These include small, 0.55kg 'cigar' sensors that are used to monitor structural movement [15], and larger microclimate sensors [16]. Some of the functionalities of these microclimate sensors include: GPS, thermal imaging, bushfire & flood detection, 360-degree camera view as well as monitoring of weather, soil, air quality and structural integrity. These capabilities are achieved using a combination of audial, optical, sonar, gas, temperature, humidity, pressure and particle sensors. Attentis devices are paired with a desktop/phone application that provides access to live data feeds for an annual subscription fee.

In 2019, Attentis created the Latrobe Valley Information Network (LVIN) at a total cost of $1,462,340 - 50% of which was funded by the Australian Government [17]. Consisting of 45 multifunction sensors (44 of which remain operational [18]), this equates to an average purchase and installation cost of $32,946 for each sensor. It is important to note that this cost does not include the recurring annual fee for access to a sensor's live data feed. At time of writing, the LVIN is the largest environmental monitoring network in existence, showcasing the full extent of Attentis' monitoring capabilities.

Until 2016, Attentis were known as 'Flamesniffer', a ground-based bushfire detection sensor company. Though no in-depth technical specifications regarding Attentis' present devices is readily available, information regarding their method of fire detection can be inferred from a patent filed by Flamesniffer in 2011 [19]. According to the patent, Flamesniffer's device used a combination of infrared (IR) pyroelectric, IR thermopile, photoelectric, and temperature sensors to detect the presence fire. The device also included a wind speed direction sensor (ultrasonic anemometer) and an ionisation smoke detection chamber. Flamesniffer's device transmitted recorded data every 1-5 minutes for 24 hours a day. The device was powered by an external solar panel and a rechargeable battery. The devices' casing had a radius of 6 inches and a height of 12 inches.

2.1.3 International Carbide Technology AB (INCA)

INCA are currently developing an AI ground-based bushfire detection sensor that pairs with an app on your phone [20]. The functionality of this sensor and it's AI algorithm is summarised in Figure 2.

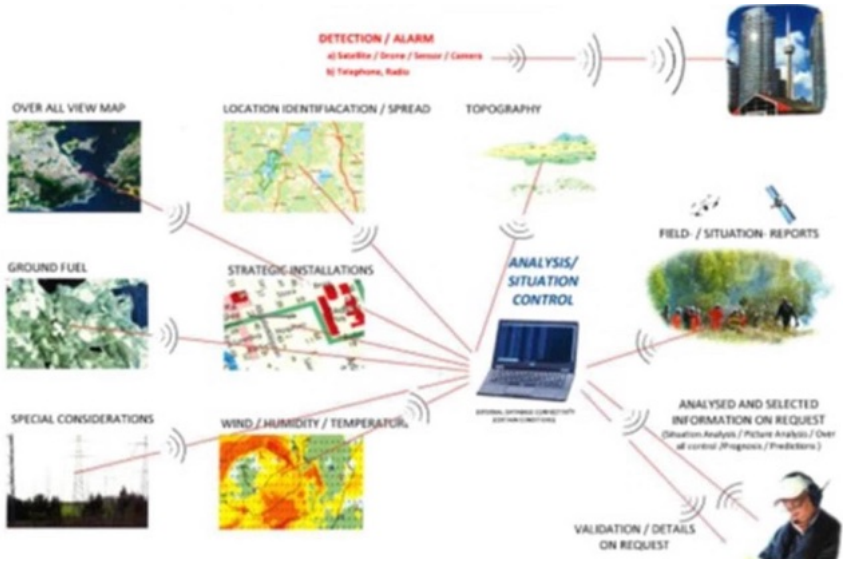

Figure 2: Functionality of INCA tech's device [21].

Though technical specifications for this sensor were not readily available, some information regarding the device's power system design requirements was identified from an internal study (Table 1) [21]. This study sought to evaluate the service life of GP CR123A Lithium Thionyl batteries and GP CR17459 Lithium Manganese Dioxide batteries. The study used four different pulses to simulate the operational power consumption of the deployed device.*

Table 1: WFS AI sensor battery design requirements [21].

Operating Voltage	Cut-off Voltage	Operating Temperature Range	Service Life	Total Lifetime Power Consumption	Cell Type	Sleep Current	Transmission Current	Sensing Current
3-5V	1.8V	-40-60C	3 years	3,200.39mAh	Primary lithium	56uA	69-125mA	3.5-14mA

Notably, INCA have opted for a primary lithium cell type, meaning there will be no energy generation functionality. The study concludes with a recommendation of four GP CR17450 Lithium Manganese Dioxide batteries wired in parallel to power the device.

2.1.4 Forest Capsule

Netherlands-based company, Forest Capsule, offer a small (approx. 15x10cm), fireproof, droplet-shaped detection device with a ten-year service life [22]. Forest Capsule devices form a mesh network that communicates through Bluetooth 5.0 and can be mass-deployed by dropping from a helicopter – their casing form ensuring they land upright. Forest Capsule's device is equipped with an accelerometer and GPS as well as: C02, temperature, smoke, wind and atmospheric pressure sensors that double as fire detection and climate change monitoring. The sensor recordings are fed into an embedded AI layer that estimates the risk of a potential fire. The devices are powered by a 14mAh industrial battery that is charged by a 4x4cm solar panel. Despite these impressive specifications, there are no verifiable deployments of Forest Capsule's sensor.

2.1.5 Green Triangle Fire Alliance and Working on Fire Australia

The Green Triangle is one of Australia's major forest regions, spanning some 6 million hectares surrounding Mt. Gambier in South Australia [23]. The Green Triangle Forest Industries Hub (GTFIH) consists of roughly 90% of forest plantation entities in the Green Triangle, who paired together under one lobbying organisation. In 2018, the GTFIH received funding from the Federal Government as a part of the "Growing a better Australia" initiative [24]. The primary goals of the GTFIH are centred around ensuring a prolific future for the Green Triangle forest industry [23]. In 2020, Working on Fire Australia received $55,000 from the GTFIH to replace two decommissioned fire watcher towers with their Firehawk detection system. The Firehawk detection system consists of a 360-degree view camera atop a 25-metre-high tower. The camera feed produces infrared (IR) heat detection vision which is fed into an AI fire detection system [25]-[26]. In 2021, this same detection system was also deployed for testing in Tasmania [27].

* The full methodology of the study can be found in Appendix D

2.1.6 Pyreos

Scotland-based manufacturer, Pyreos, sell low-cost IR pyroelectric detectors that are primarily used in industrial safety applications [28]. More specifically, two of Pyreos' three flame detection sensors claim to have applications in forest protection - the Digital and Analog TO-39 [29]. Despite this claim, no verifiable deployments of these sensors in a forest protection context were identified. The Digital and Analog TO-39 IR pyroelectric sensors have respective operating currents of 3.5-23uA and 65uA, as well as maximum respective detection ranges of 85m and 65m. The Digital TO-39's superior detection range, signal-to-noise-ratio, lower operating current and "sleep mode" functionality make it the preferred candidate for remote bushfire detection applications.*

In 2021, in collaboration with UK optoelectrical firm, Tethir, Pyreos received a £500,000 grant from Innovate UK to produce a commercially viable ultra-low power fire monitoring system for power companies [30]. Together, Tethir and Pyreos are seeking to use this funding to develop a solution for rapid detection of wildfires that occur due to fallen power lines. These fires are often devastating because they typically occur in high windspeeds. More specifically, Tethir hopes to use their optical experience to greatly improve the detection range of Pyreos sensors by more than an order of magnitude (to about 1.7km).

2.1.7 Parallel Flight Technologies

Parallel Flight Technologies (PFT) are a Californian company seeking to develop a drone with a heavy-load flight time an order of magnitude longer than present technology. This drone would double as both a bushfire detection device and a spot fire suppression tool. Currently, PFT claim to have a two-hour flight time for a 45kg payload, powered by a 5000mAh battery [31], though there are no verifiable demonstrations of this.

2.1.8 Academic papers

Finally, at an individual academic level, there have been numerous papers written investigating the viability of different ground-based fire detection sensor mechanisms [32]-[34]. For example, Dampage U. et al. use an Arduino Nano microcontroller, nrf24L01 transceiver module, DHT22 temperature and humidity sensor, light-dependent resistor and MQ9 carbon monoxide sensor to create a bushfire detection mesh network sensor node powered by four coin cell batteries [30]. Through 7000 data samples from 15 controlled fire, their device was found to have a maximum reliable detection radius of 5m. Ultimately, the authors found the device to be an effective method of early fire detection if paired with a secondary solar panel power supply.

2.2 Energy Harvesting for IoT

Section 1.2 of the literature review successfully identifies several potential power sources utilised by existing ground-based bushfire detection devices. This subsection seeks to identify any additional methods of energy generation utilised by existing IoT sensor networks that may have potential applications in remote bushfire detection devices.

* A comprehensive comparison of these two sensors may be found in Appendix E

2.2.1 Thermoelectric Energy Harvesting

The thermoelectric effect refers to the process by which a temperature difference across position can be used to generate an electric current.

Thermoelectric generators are commonly used to improve efficiency in systems with large amounts of wasted heat energy. Numerous papers have been published discussing the viability of thermoelectric energy harvesting [35]-[36]. The primary limitation regarding thermoelectric energy as a power source is output power. Both papers researched were only able to produce average outputs in the micro-Watt range.

2.2.2 Pyroelectric Energy Harvesting

The pyroelectric effect refers to the process by which a temperature difference across time can be used to generate an electric current.

Numerous papers have been published discussing the viability of pyroelectric energy harvesting [36]-[37]. Similar to thermoelectric energy harvesting, the primary limitation regarding pyroelectric energy as a power source is output power. Both papers researched were only able to produce average outputs in the micro-Watt range.

2.2.3 Radio Frequency (RF) Energy Harvesting

RF energy harvesting refers to the process by which electromagnetic waves may be converted to electrical power.

Numerous papers have been published discussing the viability of RF energy harvesting [38]-[39]. The primary limitation regarding RF energy harvesting is drop-off in power generation as the distance between transmitter and receiver is increased.

3 Component Analysis

This section uses the findings of the literature review to compile a list of components with demonstrated applications in a ground-based bushfire detection device. Where applicable, an investigation is conducted into the power consumption of existing commercially available products. All components identified in this section have a minimum of three distinct operating modes: “Sampling”, “idle/standby”, and “sleep”. For each of these modes, the maximum instantaneous current consumption is recorded from the cited datasheets. Where applicable, a brief explanation is given explaining a components relevance to fire detection (i.e. associated detection method).

3.1 Transceiver

A fundamental component of any remote sensing device is a transceiver module. Transceivers facilitate the transfer of information between device and operator. This section will specifically focus on radio transceivers.

Radio transceivers use an antenna to generate and receive radio waves of a specific frequency band. Such transceivers are responsible for the cellular reception (3G and LTE) that enables phone calls, video chats and general smartphone internet connectivity. In Australia, specific frequency bands are licensed to cellular providers by the government for a fee [40]. This prevents the interference of signals between two providers operating on the same frequency band.

Traditional methods of cellular communication are optimised for higher data transfer rates and long signal range at the cost of increased power consumption. With the advent of IoT, numerous new methods of cellular communication have emerged that prioritise low power consumption over high data transfer rates. Some of these include: LoRa, Bluetooth 5.0, Sigfox, MIoTy and NB-IOT. This paper will specifically focus on LoRa communication.

LoRa is a patented wireless communication method that was acquired and commercialised by Semtech in 2012 [41]. LoRa combines chirp spread spectrum frequency modulation with an adaptive data rate and adaptive power level to achieve ultra-low device power consumption while still maintaining a relatively long effective signal range [42]. Typical transmission range of LoRa transceivers is between 12-15km [43].

LoRaWAN is a networking protocol specifically designed for IoT applications. LoRaWAN defines the system architecture and communication protocol for a LoRa-based communication network [43]. The primary limitation of LoRaWAN communication network is a lack of existing infrastructure. As such, LoRaWAN deployments generally require the construction of custom network infrastructure.

IoT applications commonly deploy devices in a mesh networking configuration. As identified in the literature review, it is also common to deploy ground-based bushfire detection sensors in a mesh network configuration. The primary benefits of a mesh network configuration are reduced average device cost and power consumption. These benefits stem from the need for only one long range transceiver (gateway) to communicate with many devices (Figure 3).

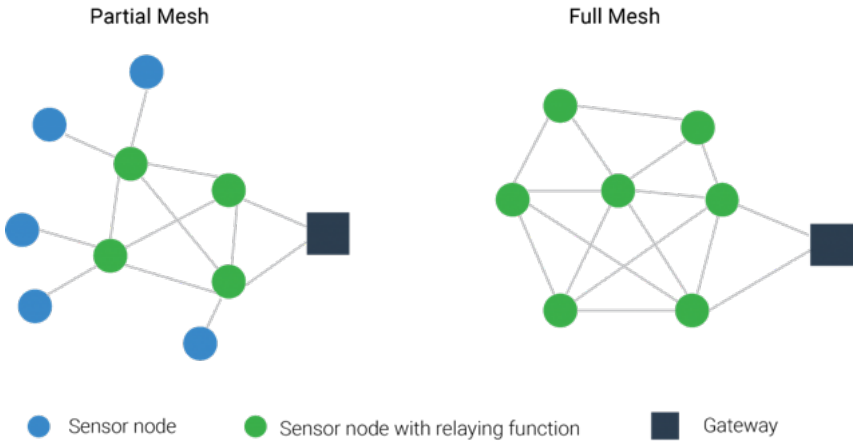

Figure 3: Example mesh network topology [44].

A 2017 study by L. Casals et al. conducts a comprehensive literature review on the power consumption of existing commercially available LoRaWAN modules. The authors literature review characterises each module based on its average current consumption in "sleep", "transmit" and "receive" operational modes (Table 2).

Table 2: L. Casals, et al. literature review examining power consumption of existing LoRaWAN modules [45].

Transceiver	Current Consumption		
	Sleep	Transmit	Receive
Semtech SX1272 [33]	0.1 µA (max. 1 µA)	Min.: 18 mA (7 dBm) Max.: 125 mA (20 dBm)	10.5 or 11.2 mA
Semtech SX1276 [34]	0.2 µA (max. 1 µA)	Min.: 20 mA (7 dBm) Max.: 120 mA (20 dBm)	10.8, 11.5 or 12.0 mA
HopeRF HM-TRLR-LF/HFS [35]	2 µA (min. 1.2 µA, max. 3 µA)	Min.: 35 mA (13 dBm) Max.: 120 mA (20 dBm)	16 mA (min. 15 mA, max. 18 mA)
Microchip RN2483 [36,37]	Up to 100-150 µA	Min.: 17.3 mA (−4.0 dBm) Max.: 38.9 mA (14.1 dBm)	14.2 mA

The papers authors go on to highlight how the traditional characterisation of current consumption by "sleep", "transmit" and "receive" provides an inaccurate representation for a LoRaWAN module and identify eleven distinct operating stages with which power consumption may be more accurately modelled. Despite these findings, due to scoping, this paper will only consider "sleep", "transmit" and "receive" modes when modelling operational power consumption.

3.2 Microcontroller

Another core component of any x(sensing device) is a microcontroller unit. The microcontroller can be thought of as a brain that controls the physical operations of all of a device's components. The microcontroller also translates information between sensors and the transceiver before it may be broadcast back to an operator.

The topic of microcontrollers is an incredibly dense and broad information space. Due to scoping, this paper will not include any detailed investigation into the viability of specific microcontrollers in an IoT bushfire detection sensor network application. Instead, the paper will only examine the ST Microelectronics STM32L496xx. As such, it is important for readers to note that it is possible there are better, more optimised alternatives available. The operational supply current of the STM32L496xx is summarised in Table 3.

Table 3: Power consumption of ST Microelectronics STM32L496xx microcontroller [46].

Microcontroller	Sleep Supply Current (nA)	Idle Supply Current (nA)	Active Supply Current (uA)	Power Up Time (s)	Cost (AUD)
ST M32L496xx	25	108	97	0.00001	12.28

3.3 Temperature Sensor

Temperatures within a bushfire can be anywhere within the range of 600°C to 1600°C [48]. Thus, there are obvious applications for a temperature sensor in the detection of a bushfire. The literature review identified multiple other, less obvious applications of a temperature sensor in a fire detection context. These include: monitoring the intensity across different regions of an active fire and monitoring ambient temperature to predict the risk of fire ignition.

There are numerous types of temperature sensors utilising different methods of temperature detection. Some of these include: thermistors, thermocouples, thermopiles, resistance temperature detectors and semiconductor-based (integrated circuit) temperature sensors [49].

All applications of temperature sensors identified in the literature review used thermopiles as their chosen method of detection. In a fire detection and monitoring application, this makes sense as thermopiles have the greatest detection range of all temperature sensors. Accordingly, this paper will specifically focus on thermopiles.

When seeking to understand the functioning of a thermopile, one must first examine thermocouples. Thermocouples produce a non-linear temperature-dependent voltage difference that may be interpreted (often using a lookup table) to measure temperature [50]. The behaviour of thermocouples is described by the Seebeck effect.

The Seebeck effect is a thermoelectric phenomenon that describes the electromotive forces (EMF) generated across two points on a conductor with different respective temperatures. A thermocouple measures the voltage at the interface of two electrically dissimilar conductors to achieve a wider effective detection range than is possible with just one material. The primary limitation of thermocouples is detection accuracy. Despite this, thermocouples are capable of monitoring a much greater range of temperatures than other temperature sensors.

Thermopiles consist of multiple thermocouples connected in series. This results in an even wider effective detection range than is possible with a single thermocouple.

Accordingly, information on the power consumption of several existing commercially available temperature sensors (Table 4) was gathered as to ensure an accurate representative sensor was chosen for final calculations.

Table 4: Power consumption of various thermocouple temperature sensors.

Temperature Sensors	Sleep Supply Current (uA)	Standby/Idle Supply Current (uA)	Sampling Supply Current (uA)	Sampling Time (ms)	Power-up/down Time (ms)	Source
AMS AS621x Series	<0.1	9	16	51	150	[51]
Sensirion STS4x Series	N/A	3.4	500	8.3	1	[52]
Bosch BME680	1	0.8	1	unspecified	2	[53]

3.4 Humidity Sensor

A side effect of the increased temperatures produced by a bushfire is a reduction in relative humidity. On it's own, a humidity sensor is of little use in the detection of a bushfire, however, N, Varela *et al.* uses a humidity sensor in conjunction with a temperature sensor to detect the presence of a fire with 100% efficacy [54]. Though no specifics are given on the detection range and threshold, the authors paper serves as a proof of concept that, when used in conjunction, these sensors offer an effective method of fire detection. Additionally, information on ambient relative humidity can be used to predict the risk of fire.

There are numerous types of humidity sensors utilising different working principles. By broadest differentiation, humidity sensors are classified as either relative or absolute humidity sensors. Relative humidity sensors record the humidity of the air at a given temperature in proportion to the expected humidity in the air for the given temperature. Absolute humidity sensors record the actual amount of water vapour per unit gas. This paper only considers relative humidity sensors.

Information on the power consumption of several existing commercially available humidity sensors (Table 5) was gathered as to ensure an accurate representative sensor was chosen for final calculations.

Table 5: Power consumption of various temperature and relative humidity sensors.

Temperature & Relative Humidity Sensor	Sleep Supply Current (uA)	Idle Supply Current (uA)	Sampling Supply Current (mA)	Sampling Time (ms)	Power Up Time (ms)	Source
Sensirion SHTC3	0.6	70	0.57	0.8	0.24	[55]
DHT11	N/A	150	2.5	15	0.08	[56]
Sensirion SHT3x	N/A	45	1.5	15	0.5	[57]

3.5 Gas Sensor

When a piece of wood is partially burnt, a byproduct of the incomplete combustion is smoke. This smoke is comprised of several gases including: evaporated water (steam), CO2, CO, etc. [59].

On the molecular level, many of the gases in bushfire smoke are produced as a result of the heating of volatile organic compounds (compounds which evaporate easily when heated). For example, the sap and cellulose within a tree are comprised of hydrocarbons that evaporate when heated. When all of the volatile organic compounds (VOCs) are burnt off, all that is left is charcoal, which, when burnt, will combine with oxygen to release CO2.

The smoke released by a bushfire is of great promise in early detection applications. This is because a fire will typically exist in a smouldering phase for up to an hour before actually igniting [11]. Thus, gas sensors present a promising solution for the early detection of fires. The literature review confirms this analysis, finding that many commercial ground-based bushfire detection sensors utilised a gas sensor as a method of detection.

Several different methods of smoke detection exist. The literature review identified use cases in a bushfire detection application for three types of smoke detectors: a VOC gas sensor, an ionisation chamber and a photoelectric detector. These are discussed in greater depth in the following subsections.

3.5.1 VOC Sensor

The working principles of a VOC sensor vary substantially between different manufacturers. This paper will specifically focus on photoionisation VOC detectors as they are widely regarded as the cheapest and most abundant VOC sensor [60]. Photoionisation detectors use ultraviolet light to ionise VOCs. Each VOC has an ionisation potential value, which represents the energy required to liberate an electron. Thus, by monitoring the intensity of the incident ultraviolet light and the conductivity of the air within the sensor, one may detect the presence of a VOC. Photoionisation detectors are a relative VOC sensor, meaning they cannot detect the absolute quantity of a detected VOC.

Information on the power consumption of some existing commercially available VOC sensors (Table 6) was gathered as to ensure an accurate representative sensor was chosen for final calculations.

Table 6: Power consumption of various VOC sensors.

VOC Sensors	Sleep Supply Current (uA)	Standby/Idle Supply Current (uA)	Sampling Supply Current (uA)	Heating Supply Current (mA)	Heating Time (ms)	Sampling Time (s)	Power Up Time (ms)
Bosch BME680	1	0.8	90	13	300	92	2
Sensirion SGP40	N/A	105	4000	Included in sampling current	Included in sampling time	60	0.6

3.5.2 Photoelectric Detector

A photoelectric detector consists of a PN junction that generates a charge when struck by incident photons [19]. The background phenomenon behind the working principles of a photodetector is the photoelectric effect.

A photodetector may be contained in a chamber with an LED to create a smoke detector. In this configuration, the LED is mounted such that it is not shining directly onto the photoelectric detector. When the chamber fills with smoke, the diffraction of light from the LED is registered by the photoelectric detector.

Information regarding the power consumption of existing commercially available ionisation chamber smoke detectors was not collected as they are of little value for early detection in comparison to VOC smoke detectors.

3.5.3 Ionisation Chamber

Another method of smoke detection identified in the literature review is through the use of an ionisation chamber. An ionisation chamber consists of a chamber containing two electrodes (an anode and a cathode) and a small quantity of radioactive material [19]. The chamber is filled with air and a potential difference is applied to the electrodes, forming an electric field. When atmospheric gas particles are ionized by the radioactive material, a flow of charge develops between the two electrodes. When smoke enters the chamber, the conductivity of the chamber's air decreases, resulting in a reduction of current [62].

Information regarding the power consumption of existing commercially available ionisation chamber smoke detectors was not collected as they are of little value for early detection in comparison to VOC smoke detectors.

3.6 Image-based Detection

Within the literature review, infrared and visible light imaging systems were identified in bushfire detection applications. Images captured by these systems may be digitised and passed through image processing algorithms to detect the presence of fire.

3.6.1 Visible Light Camera

A camera module consists of three basic components: a lens, an image sensor and an image signal processor. Incident light is focused onto the image sensor by the lens and then interpreted into a digital image by the image signal processor.

A visible light camera refers to a camera which is optimised to detect visible light waves (380-750nm). While no commercial use cases were identified for visible light cameras, research was found identifying their viability as a bushfire detection method. Among these identified includes a thesis completed in 2021 by H. Kaur [34]. Kaur uses colour and motion detection as well as frequency domain analysis to detect the presence of a fire

(Kaur notes that background subtraction algorithms may also be used in fire detection analysis). Through the use of these algorithms, Kaur was able to achieve a detection efficacy rating of 99.17%. It is important to note that the source videos used to evaluate this detection system were stock videos of novel fires (not bushfires). Despite this, Kaur's paper proves the potential viability of a visible light imaging bushfire detection system.

An attempt was made to gather information on the power consumption of several existing commercially available visible light camera modules, however, reliable data was ultimately too difficult to ascertain.

3.6.2 Thermal Imaging Camera

All objects with heat energy emit thermal radiation (even ice). If a system has sufficient energy, it may even emit visible light (e.g. fires). Thermal imaging detection cameras use image sensors that detect the presence of infrared light (IR). Given IR's longer wavelength (relative to visible light), thermal imaging sensors have larger pixel dimensions that produce lower quality images. However, thermal imaging is superior to visible light in its abilities for detection during the night and in harsh weather conditions. For example, the longer wavelength of IR light allows it to pass through smokey conditions where visible light will be scattered and absorbed [63]. As such, thermal imaging cameras are of great interest when detecting the presence of a fire. The literature review confirms this analysis, finding several use cases of thermal imaging cameras in commercial ground-based bushfire detection sensors.

An attempt was made to gather information on the power consumption of several existing commercially available visible light camera modules, however, reliable data was ultimately too difficult to ascertain.

3.7 Pyroelectric Detector

Pyroelectric detectors are a form of thermal detector that operates using the pyroelectric effect. The pyroelectric effect is closely related to thermoelectricity, whereby incident IR light generates a flow of heat energy through a ferroelectric crystalline material, producing an electric change across the crystal [64]. In a pyroelectric detector, the electric change is measured across electrodes either side of the ferroelectric material. If the change in temperature of the material is permanent, the generated potential difference will eventually fade away due to the inherent behaviour of the ferroelectric material.

The pyroelectric effect is closely related to the piezoelectric effect. More specifically, primary pyroelectricity refers to the electric change generated by the contraction and elongation of dipoles within the crystal [65]. Secondary pyroelectricity refers to electric change generated by piezoelectricity that is generated by stresses caused by the thermal expansion of dipoles.

The literature review identified multiple applications of pyroelectric detectors in a fire detection context. More specifically, Attentis use IR pyroelectric detectors to observe the C02 signature of fire flames and embers. Attentis accomplishes this through the addition of two filters [19]. The first filter (0-4200nm) eliminates the spectral signature of the sun, while the second filter (4500-7000nm) eliminates false alarms triggered by motion. The resulting bandpass filter (4200-4500nm) is specific to the spectral signature of C02 (Figure 4).

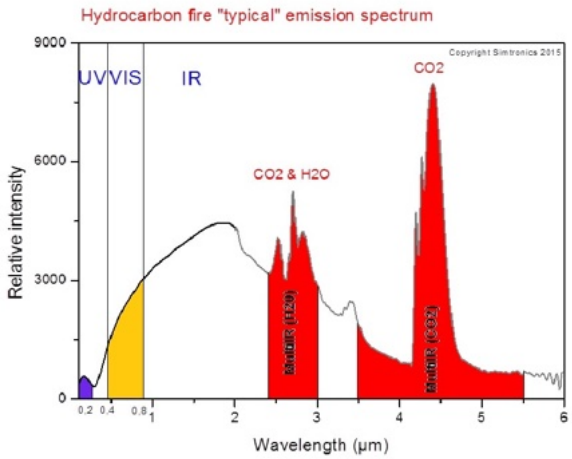

Figure 4: Hydrocarbon fire "typical" emission spectrum [66]

The power consumption of a pyroelectric detector is highly dependent on the external circuitry. Accordingly, it is rare for manufacturers to include information on power consumption in datasheets. Thus, it was not possible to gather information on the power consumption of existing commercially available pyroelectric detectors.

4 Device Configurations

This section uses the literature review and components analysis sections to compile a list of possible detection methods (i.e. combinations of sensors) which may be used in a ground-based bushfire detection device. The lifetime power consumption of each detection method is calculated for various sampling frequencies.

It is clear that a plethora of sensors may be used in the detection and monitoring of a bushfire. From the eight detection methods identified by the literature review, there are thousands of possible combinations. Obviously, it is unrealistic for this work to consider lifetime power consumption for all of of these possible combinations. Instead, this section will perform calculations for the two extremes to develop an idea as to the total range of lifetime power consumption. Calculations will also be performed for some of the detection methods identified in the literature review (Table 7). Despite these limitations, it would be trivial for someone to use the method outlined above to perform lifetime power consumption analysis for a sensing combination of their choosing.

Research conducted in the literature review indicates it is common for ground-based bushfire detection sensors to be deployed in a mesh network configuration. A mesh network implies that deployed devices communicate with one another. The primary benefit of a mesh network configuration is a reduction in power consumption. By using a mesh network, individual sensing devices need only be able to communicate with the closest device, meaning transmission distance (and thus, power consumption) is greatly reduced. To facilitate communication with an operator, a larger gateway device with a longer transmission range is used. Accordingly, this section of the report assumes devices are deployed in a mesh network configuration with negligible distance between each device. Thus, distance of transmission is not considered in device lifetime power consumption calculations.

Finally, the literature review identified that lifetime power consumption may further be reduced by the use of a risk prediction matrix that only activates certain sensors based

on detection thresholds. This report will not consider this method of power reduction.

Table 7: Device configurations.

Sensor Configuration	Sleep Supply Current (uA)	Sampling Supply Current (mA)	Sampling Time (s)	Idle Supply Current (uA)	Power Up Time (s)	Packet Size (bits)	Cost (AUD)	Source
Sensirion SHTC3 (temperature and humidity)	0.6	0.57	0.0008	70	0.00024	154	4.74	[56]
Bosch BME680 (temperature, humidty, pressure and gas)	1	0.09	92	0.8	0.002	150	22.26	[61]
Sony IMX335 Camera Module (visible light)	N/A	150	15	N/A	N/A	2.6E+07	40	[67]
Sony IMX335 Camera Module (IR)	N/A	150	15	N/A	N/A	2.6E+07	40	[68]
T5919 (audial)	0.009	0.00022	15	0.22	0.007	1440000	2.95	[69]
ePR44xx2 (pyroelectric detector)	0.023	0.000023	1	0.023	N/A	300	100.1	[29]

4.1 Method

The values outlined in Table 7 were read into a Python script (see Appendix G) and used to calculate the operational lifetime power consumption for each device configuration. In short, each sampling current was multiplied by the sampling time and sampling frequency. This value was added to the idle/standby supply current multiplied by the power up time and the sampling frequency. For the remainder of a day, the device was considered to be in sleep mode. Similar calculations were performed for the microcontroller and added to the lifetime power consumption value for each device configuration. Finally, the packet size for each device configuration was divided by the transmission bit rate and multiplied by the transmission supply current to calculate power consumption due to transmission. The full Python script written to perform these calculations can be found in Appendix G.

4.2 Results

The same method as outlined above was used to calculate the lifetime power consumption for each device configuration. The sampling frequency and intended operational lifetime were modified to create a total of six different examples.

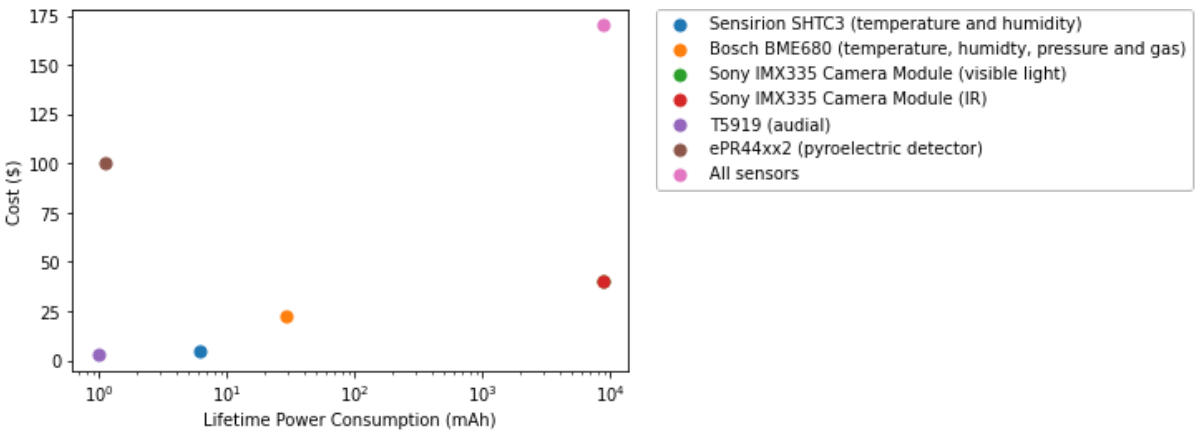

Figure 5: Lifetime power consumption of sensor configurations at a sampling rate of one sample per hour for one year.

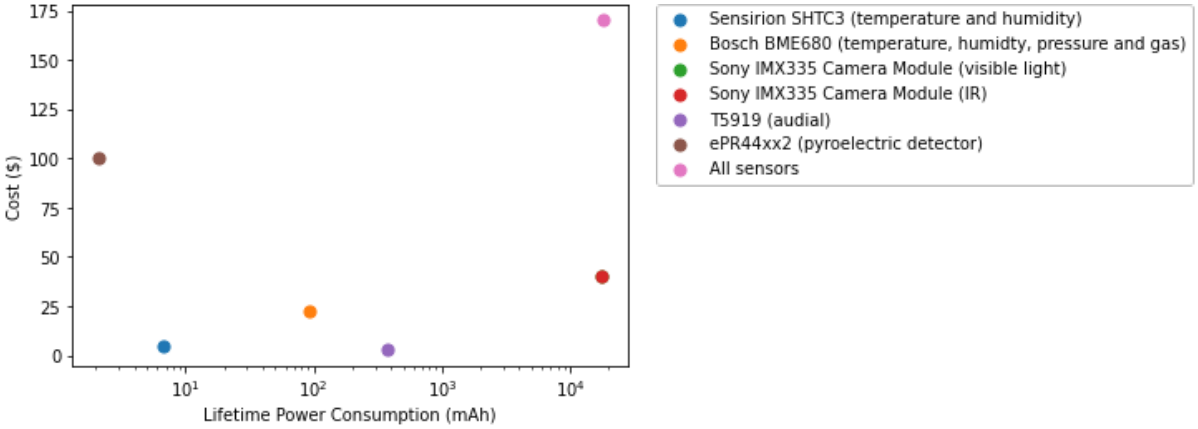

Figure 6: Lifetime power consumption of sensor configurations at a sampling rate of two samples per hour for one year.

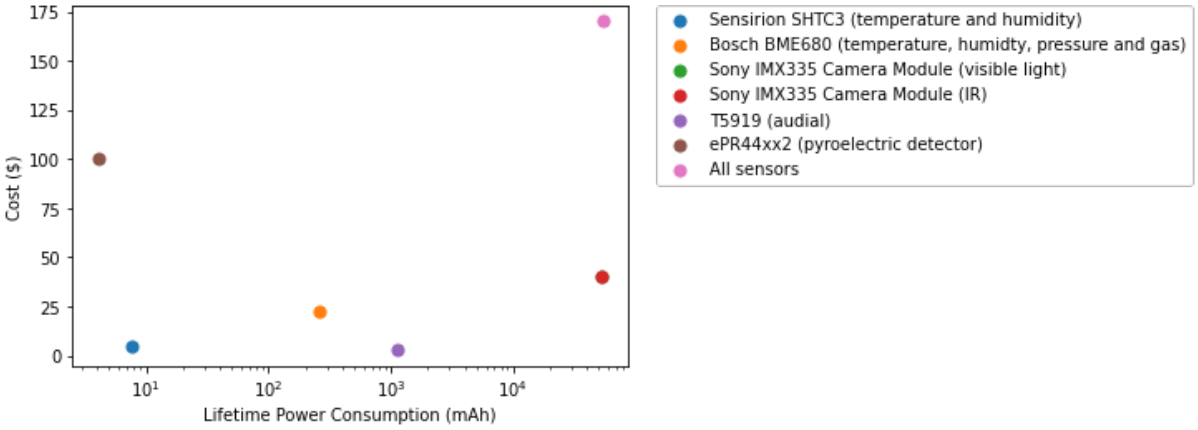

Figure 7: Lifetime power consumption of sensor configurations at a sampling rate of six samples per hour for one year.

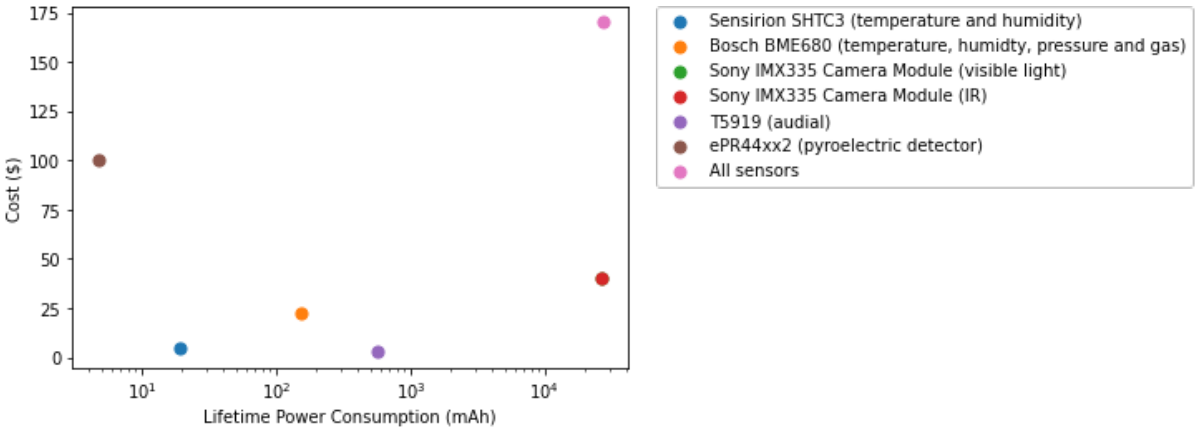

Figure 8: Lifetime power consumption of sensor configurations at a sampling rate of one sample per hour for three years.

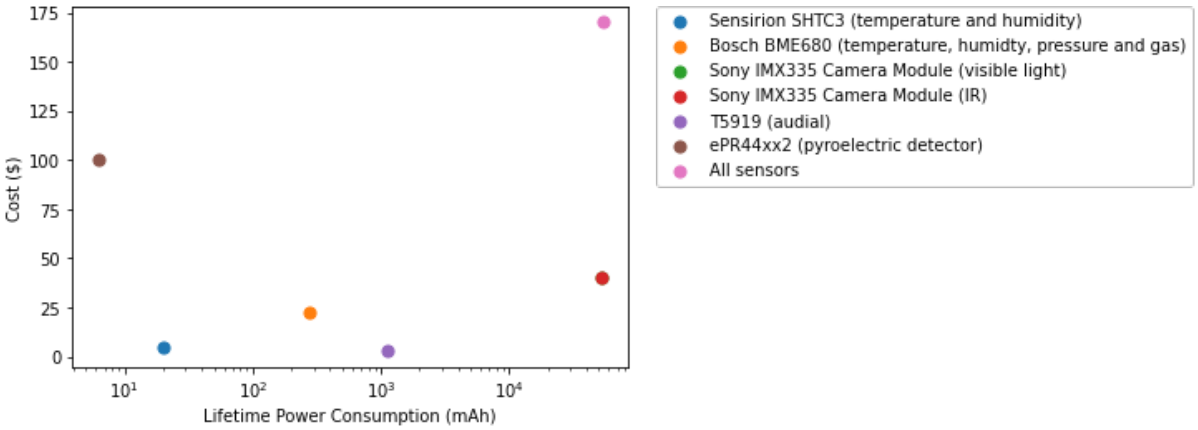

Figure 9: Lifetime power consumption of sensor configurations at a sampling rate of two samples per hour for three years.

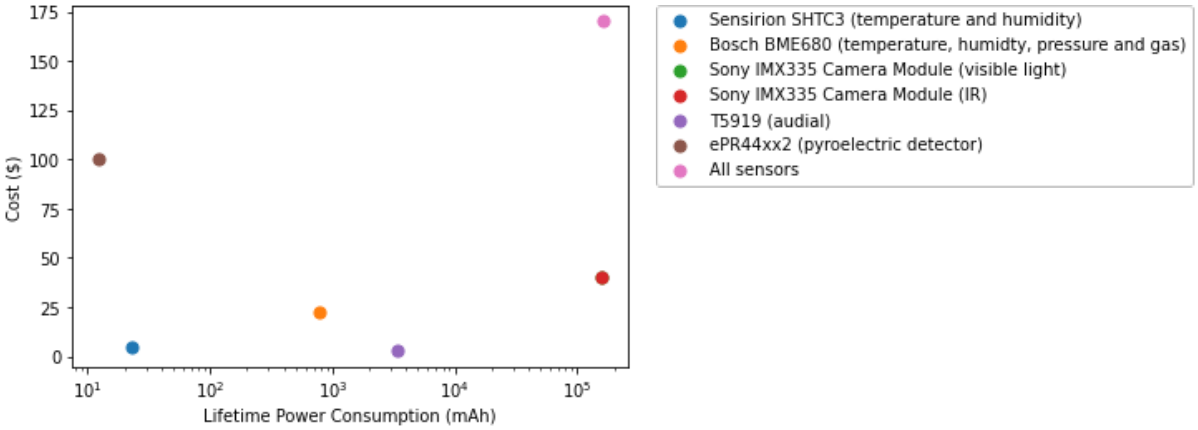

Figure 10: Lifetime power consumption of sensor configurations at a sampling rate of six samples per hour for three years.

5 Potential Power Supplies

This section will evaluate different potential power supplies as to make a recommendation for each of the developed lifetime power consumption graphs. The power sources discussed in this section were sourced from research done in the literature review.

5.1 Batteries

A battery is a device that stores chemical energy, converting it into electricity. The mechanism underpinning this conversion of energy is called an electrochemical cell. Electrochemical cells consist of two electrodes (an anode and a cathode) separated by an

electrolyte. The flow of charge through an electrochemical cell is explained by redox reactions [70].

When analysing the lifetime of a battery, it is important to consider both the battery's capacity, and how the battery is discharged. In a perfect energy storage system, lifetime may be calculated by dividing the capacity (in $amperes \times hours$) by the average current consumption ($amperes$). In a real energy storage system, there is energy leakage dependent on the instantaneous rate of discharge. The internal circuitry of an energy storage device is usually optimised by manufacturers for a specific rate of discharge that minimises these losses and gives the battery a lifetime as advertised.

S. Farahani explains these losses writing, "Losses due to the instantaneous rate of discharge may be explained by the relaxation phenomena (or recovery effect). When a battery is discharged at a high and sustained rate, the battery reaches its end of life even if there are still active materials left in the battery. However, if the discharge rate is not continuous and there are cutoffs or very low-current periods, the transport rate of active materials catches up with the depletion rate of materials, giving the battery a chance to recover the capacity lost at the high discharge rate" [71].

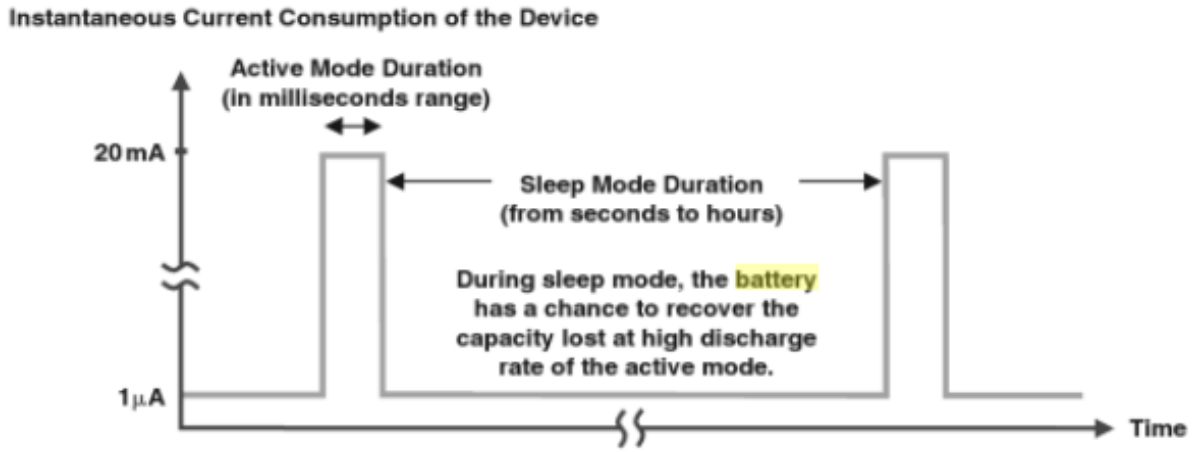

Figure 11: An example current profile of a device in a wireless sensor network [71].

If the power requirements of the external circuitry allow it, an appropriately large capacitor may be used to entirely decouple the battery from periods of high instantaneous current consumption. In this case, the battery charges the capacitor while the device is asleep and the external circuitry draws charge from the capacitor when instantaneous current consumption is high.

Thus, there are two approaches to ensuring a battery will perform in accordance with design specifications. Firstly, the external circuitry may be designed with a capacitor such that the instantaneous discharge rate of the battery is never greater than that which is specified by the manufacturer. Alternatively, the true battery efficiency for a specific use case must be determined. This may be done experimentally, or by contacting the battery manufacturer and supplying them with a simplified model of the device's instantaneous current consumption. This work assumes that the circuitry of a device is designed such that it does not surpass the battery's maximum instantaneous discharge rating.

5.1.1 Primary Cell

A primary cell is a type of electrochemical battery with no recharging functionality. These batteries tend to be of low cost with long lifetimes. Primary cell batteries are generally seen as environmentally unfriendly, requiring 50x more energy to produce than they my store [72].

5.1.2 Secondary Cell

A secondary cell refers to a battery with recharging functionality. These batteries tend to have a higher initial cost and a larger form factor than primary cell batteries, however, they also have a greatly increased lifespan. Secondary cells are recharged by passing charge through the battery terminals in the opposite direction to discharging.

5.2 Super Capacitor

A super capacitor refers to a capacitor with a much higher capacitance value than a traditional capacitor. Super capacitors have an energy density up to two order of magnitude greater than traditional capacitors, can accept and deliver charge much faster than batteries and tolerate many more charging cycles than secondary cells [73].

There are two types of super capacitors: double-layer electrical capacitors (EDLC) and pseudocapacitors.

EDLC use electrostatic attraction to intercalate charges at the interface between electrodes and electrolyte. Thus, EDLC do not involve any chemical reactions. Typically, EDLC have a high power density, fast charging and long lifetimes [ref].

Pseudocapacitors use faradaic reactions to store charge at electrodes. Typically, pseudocapacitors have a higher energy density than EDLC but shorter lifetimes and lower power densities.

5.3 Photovoltaic Panels

Despite investigating multiple methods of energy harvesting, the literature review identified photovoltaic (PV) panels as the only presently viable method of energy harvesting for a remote bushfire sensing application. PV panels convert photons into electrons. The phenomenon behind this conversion of energy is known as the photoelectric effect. More specifically, PV panels consist of a semiconductor that is particularly sensitive to the photoelectric effect when exposed to sunlight. These semiconductors form junctions with an electrically dissimilar material where a thin electrical barrier is used to separate charge. Materials are selected such that they optimise the PV panels efficiency, cost and form factor.

Typical efficiency for commercially available solar panels is within the 20% to 30% range [74]. According to J. Geisz et al., this is because PV panels constructed with a single semiconductor (junction) are "fundamentally limited" to efficiencies of about 30% due to the Shockley-Queisser limit. Losses in efficiency of PV panels are primarily driven through non-radiative recombination. Notably, researchers have achieved efficiencies as high as 47.1% [74] by combining multiple junctions into a single solar cell. Theoretically, efficiency may be as high as 87% as the number of junctions approaches infinity.

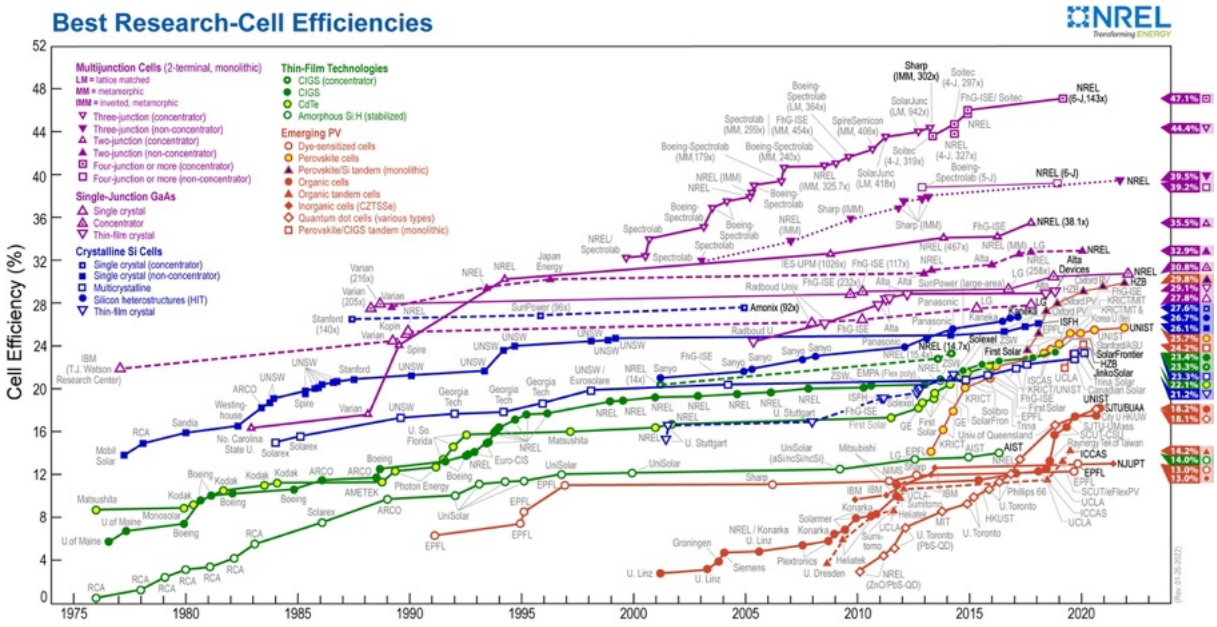

Figure 12: Efficiency of different solar cells as tracked by NREL [75].

5.3.1 First Generation Solar Cells

First generation solar cells are constructed using crystalline silicon (c-Si). They are the cheapest and most common type of solar cell accounting for roughly 90% of the total market share for all solar cells [76]. Typical efficiency for c-Si solar cells is around 20%.

5.3.2 Thin-film Solar Cells

Thin film solar cells are a second-generation solar cell that is made by depositing a thin film of PV material atop a substrate [77]. Thin-films may encompass a considerable range of thickness, varying from a few nanometres to several micrometres. Some thin film PV panels are cheaper than first-generation solar cells, but they were also less efficient. Recent breakthroughs in PV panel technology has seen the efficiency of for more expensive thin-film PV panels climb to values similar to that of first-generation solar cells.

Due to the smaller amount of PV material used in a thin-film panels (relative to first generation solar cells), they are generally seen as more environmentally friendly. Despite this, thin-film solar cells use two panes of glass (whereas first-generation solar cells only use one), making them approximately twice as heavy as first-generation cells.

As indicated by Figure 12, the most efficient solar cells produced to date consist of several thin-film solar cells layered atop one another to form a multi-junction solar cell. Despite this, thin-film PV panels have failed to capture a majority market share due to their expensive materials and manufacturing processes.

For example, consider gallium arsenide (GaA) thin-film PV panels. GaA is a binary metal that is widely agreed upon as the best-performing semiconductor for a thin-film solar cell. This is due to their exceptional heat resistance properties and high efficiency. In 2019, researchers M. Green *et al.* created a GaA thin-film solar cell achieving an efficiency of 29.1% - very close to the theoretical limit for single-junction solar cells. Despite this, GaA solar cells are limited in their commercialisation due to their expensive material

costs. Presently, GaA solar cells only see industrial use in industries such as space travel or in concentrator solar cells.

5.4 Results

Research conducted in this section indicates that first generation solar cells are a more viable source of energy generation than thin-film solar cells. Further research is needed to determine whether a secondary cell is preferential to supercapacitor.

Though a specific value of device power consumption where primary cell batteries become economically enviable was not defined, research indicates that primary cell batteries are a feasible power source for all device configurations except those including visual detection methods. While it may be possible to use a primary cell battery for a visual-based detection device with an operational lifetime of one year, it is certainly economically inviable for operational lifetimes greater than one year. In this case, a secondary cell battery or a supercapacitor should be used in conjunction with a first generation solar cell.

6 Conclusion and Future Works

Ground-based IoT sensors show major promise in greatly reducing bushfire detection times. To answer the question of how may these devices be powered, this literature review modelled the lifetime power consumption of various bushfire detection methods under different operating conditions. Research was conducted into potentially viable power sources and used to make a recommendation. The power consumption for visual-based detection methods was found to require a secondary cell battery or a supercapacitor with a solar panel, whilst primary cell batteries were found to be capable of powering all other device configurations.

The project was severely limited by a lack of publicly available information. Given that the application of IoT sensors to bushfire detection is still an infant market, there was very little information available on existing commercial products. Additionally, it was far more difficult than anticipated to obtain relevant product datasheets from manufacturers.

It should be acknowledged that the modelling of power consumption performed in the work is extremely primitive and only serves to act as a gauge as to what total range of power consumption ground-based bushfire detection sensors may fall into. All power consumption values collected in research were maximum ratings to ensure an appropriate factor of safety. For audial and optical detection methods, packet size was estimated using a file size calculator with native compression formats [78]. As such, it is important to note that these values could vary substantially.

The most flawed section of this work was the potential power sources section. In the initial scoping of this assignment, this section was intended to be used to assign specific power sources to a device configuration according to it's lifetime power consumption. This was based on the assumption that primary cell batteries would have a cost versus capacity curve similar to that represented by Figure 13.

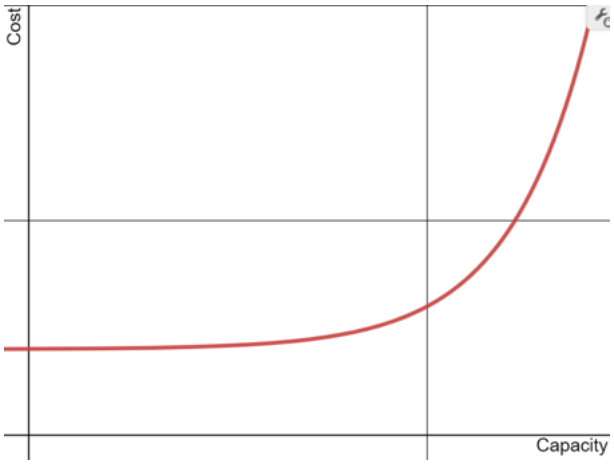

Figure 13: Theoretical cost versus capacity curve for a primary cell battery.

Intuitively, this makes sense when considering fundamental limitations of the technology. Given this assumption, it was believed that primary cell batteries would have a point of diminishing return where they become exponentially more expensive for a minimal increase in energy capacity. Such a point could be used to define the limit at which it becomes economically inviable to use primary cell batteries as an energy source. While there are many different existing studies of batteries examining cost versus year, cost versus ion, etc., there are no existing studies considering cost versus capacity. Thus, it was not possible to complete this section as initially desired.

Accordingly, data on the cost and capacity of existing commercially available batteries was collated in an attempt to research such a curve; however, it was quickly realised modelling the relationship would require a research paper of it's own. The collection of reliable information on the cost of a battery meant attaining a personalised quote directly from the manufacturer. This did not prove to be an easy feat, and so the report's focus was shifted to an examination of the power consumption of existing ground-based bushfire detection sensors.

Future research could attempt to model this relationship between battery cost versus capacity. Such a paper would be of great utility for a variety of applications not exclusive to ground-based bushfire detection sensors. Additionally, the method derived in this work serves as a model for future researchers seeking to estimate the lifetime operational power consumption of a system.

A Appendices

DRYAD

Silvanet Wildfire Sensor

Solar-powered sensor for ultra-early detection of wildfires

The Silvanet Wildfire Sensor is designed to detect forest fires during the early stages (even during the smoldering phase, within the first 60 minutes) and to monitor the microclimate, measuring temperature, humidity and air pressure. The sensor combines ultra-low-power Air Quality sensing with a precise gas sensing mode. It detects Hydrogen, Carbon Monoxide and Carbon Dioxide and other gases at the ppm level with built-in artificial intelligence in order to reliably detect a fire and avoid false positives. The sensor uses LoRaWAN communications for wireless data transmission and can run maintenance-free for 10-15 years without the need of batteries, avoiding the use of lithium and other toxic materials.

Ultra-early fire detection

- Dramatically cuts firefighting
- Prevents economical damage
- Reduces risk and insurance
- Saves human life and wildlife

Health & Growth Monitoring

- Reliable, repeatable data collection
- More effective forest planning
- Prevent diseases and fight droughts
- Optimize tree growth and ROI

info@dryad.net www.dryad.net

Silvanet Wildfire Sensor

Solar-powered sensors for ultra-early detection of wildfire

Mechanical Specification

Size	19 x 8,2 x 1,2 cm
Weight	136g
Solar Panel	6x6cm
Operational Temperature	-40℃ to +85℃
Operational Humidity	0% to 100% Condensing
Ingress Protection	IP67
Material	Plastic (Weather, UV-proof)

Regulatory Compliance

Regulatory (US)	FCC Part 15.247, 109, 209,
Environmental	ETSI EN 300 019
EMC	ETSI EN 55024
	ETSI EN 300 489

General Characteristics

Maintenance	Maintenance-free (10-15 yr)
Distance between Sensors (Radius)	100m radius for 60min detection of 2x2m fire
Sensor to Mesh Gateway (Ratio)	Typically 100 sensors per Gateway, depending on topology
Power source	Solar-powered, battery-free
Energy storage	Supercapacitors
Installation	Mounted tree (3m height recommended)

LoRa Radio Parameters

ISM Bands	NA902-928, AU915
ISM Bands	EU868, AS923
Tx Power	14 dBm

Gas Sensor Bosch BME688

Size	3.0 x 3.0 x 0.93 mm
Operation range	Pressure: 300 to 1100 hPa Humidity: 0 to 100% Temperature: -40 to 85°C
Sensors	CO, CO_2, H_2, VOC, Temperature, Humidity, Air Pressure

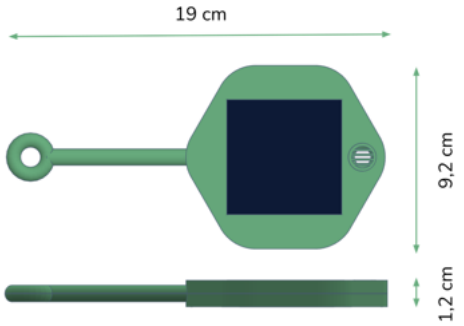

Appendix A: DWS datasheet [11].

B Appendices

DRYAD

Silvanet Border Gateway

Distributed LoRaWAN® Gateway for Large-Scale Outdoor Networks and connection with Silvanet Cloud

The Silvanet Border Gateway is placed at the border of the target forest area, typically in a forest house or near a village. The Border Gateway communicates with the Silvanet Cloud Platform, relaying messages from Wildfire Sensors (directly or indirectly via Mesh Gateways). Connectivity is provided wirelessly using the built-in LTE radio (using 4G/LTE-M with 2G/GPRS fallback) or using the built-in Ethernet adapter via a wired Internet connection. For remote deployments where there is no mobile network coverage and no access to mains power, the Silvanet Border Gateway has built-in support for satellite uplink using the SWARM satellite network. It can be operated on mains power or powered by a solar cell.

Differentiators

- Solar- or mains powered
- Built-in satellite communications (SWARM)
- Extendable to large areas with Mesh Gateway

Features

- Ethernet, 4G/LTE-M with 2G/GPRS fallback
- LoRaWAN compliant
- Firmware Update Over-the-Air (FUOTA)

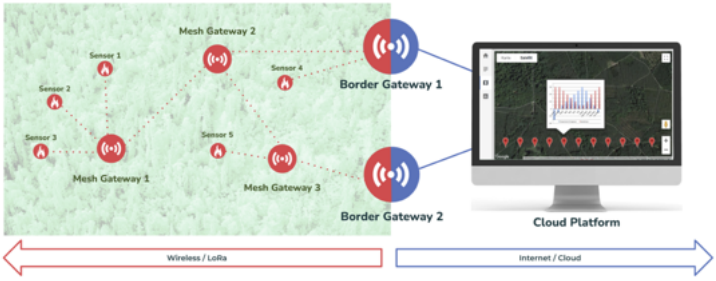

info@dryad.net www.dryad.net

Silvanet Border Gateway

Distributed LoRaWAN® Gateway for Large-Scale Outdoor Networks and Connection with Silvanet Cloud

Mechanical Specification

Size	63 x 46 x 4,5cm
Weight	1,3kg
Solar Panel	Optional, external, 67 x 36cm
Operational Temperature	-40℃ to +85℃
Operational Humidity	0% to 100% Condensing
Ingress Protection	IP64
Material	Plastic (Weather, UV-proof)

Regulatory Compliance

Regulatory (US)	FCC Part 15.247, 109, 209,
Environmental	ETSI EN 300 019
EMC	ETSI EN 55024
	ETSI EN 300 489

General Characteristics

Maintenance	Maintenance-free (10-15 yr)
Mesh Gateway to Border Gateway (ratio)	Typically 20 Mesh Gateways per 1 Border Gateway
Power source	Mains powered (PoE) or Solar panel (optional), battery-free
Energy storage	Supercapacitors
Installation	Mounted on pole or attached to a tree

Built-in Connectivity

Wired connection	Ethernet
Wireless connection	4G/LTE-M, 2G/GPRS fallback
Satellite	SWARM up- and downlink

External Connectivity

Starlink	Space X / Starlink service
Other satellite internet	VSat iFast Ku or C-Band

LoRa Radio Parameters

ISM Bands	NA902-928, AU915
ISM Bands	EU868, AS923
Tx Power	22 dBm

Receive Channels	4
Transmit Channels	1
Antenna connection	N-Type

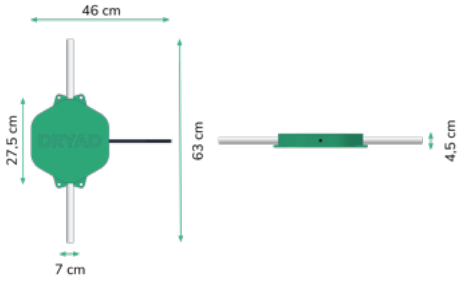

Appendix B: SBG datasheet [12].

C Appendices

DRYAD

Silvanet Mesh Gateway

Distributed LoRaWAN® Gateway for Large-Scale Outdoor Networks

The Silvanet Mesh Gateway extends the Silvanet Network to large deployments beyond the reach of the standard single-hop direct connection between sensors and gateways in standard LoRaWAN networks. The patent-pending architecture uses a multi-hop mesh network of Gateways interconnected with LoRa and each serving as a standard LoRaWAN gateway to Silvanet Wildfire Sensors and 3rd party sensors. The solar-powered Mesh Gateways are placed in the forest itself, forming a mesh network with a typical distance of 2-6 km depending on topology and physical placement of the Mesh Gateways. The Mesh Gateway only uses the LoRa radio to communicate with other Mesh Gateways or a Border Gateway. It does not require direct 4G/LTE radio or Ethernet connectivity which ensures low power consumption supported by the built-in solar panel.

Differentiators

- Extend LoRaWAN networks to large areas
- Solar-powered, maintenance-free
- Supports any LoRaWAN compliant sensors

Features

- Automatic network configuration
- Self-healing, auto fail-over mesh network
- Firmware Update Over-the-Air (FUOTA)

Silvanet Mesh Network Architecture

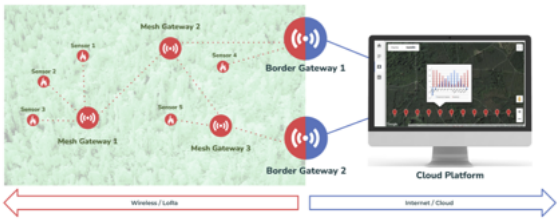

info@dryad.net www.dryad.net

Silvanet Mesh Gateway

Distributed LoRaWAN® Gateway for Large-Scale Outdoor Networks

Mechanical Specification

Size	56 x 30 x 4 cm
Weight	2,8 kg
Solar Panel	50 x 25 cm
Operational Temperature	-40℃ to +85℃
Operational Humidity	0% to 100% Condensing
Ingress Protection	IP64
Material	Plastic (Weather, UV-proof)

Regulatory Compliance

Regulatory (US)	FCC Part 15.247, 109, 209,
Environmental	ETSI EN 300 019
EMC	ETSI EN 55024
	ETSI EN 300 489

General Characteristics

Maintenance	Maintenance-free (10-15 yr)
Mesh Gateway to Border Gateway (Ratio)	Typically 20 Mesh Gateways per 1 Border Gateway
Mesh Gateway to Sensor (Ratio)	Typically 100 sensors per Gateway, depending on topology
Max distance between Mesh Gateways	2-6 km, depending on topology and placement of Gateways
Power source	Solar-powered, battery-free
Energy Storage	Supercapacitors
Installation	Mounted on pole or attached to a tree

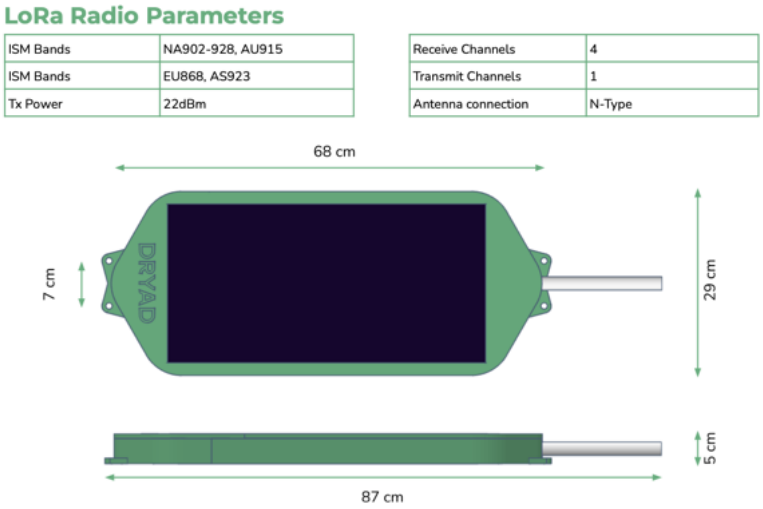

Appendix C: SMG datasheet [13].

D Appendices

Appendix: Battery Service Life Simulation

Selecting the battery is a question involving several dimensions: power, operating temperature, service life, chemistry, safety, and business (the battery needs to be commercially feasible) to mention some of the aspects.

As a part of the pre-study, information has been retrieved from GPBM Nordic regarding batteries. GPBM is a battery provider and is offering free services (as a part of their sells process) where it is possible to get information needed for the design process.

This appendix summarizes information retrieved from GPBM.

There are two possible chemistries that can be used for the sensors described, Lithium Thionyl and Lithium Manganese Dioxide. Both are common in similar applications; the Lithium Manganese Dioxide is found in both cameras and fire detectors. GPBM represents different manufacturers and provides batteries from both GP and Xeno.

The first step is to select a primary or secondary battery (non-chargeable or chargeable). In this case, a primary (non-chargeable) is chosen due to the service-life.

Given the following assumed operating condition, GPBM have assisted with simulations and tries to calculate the service life:

Voltage:	3 – 5 V
Cut off voltage:	1.8 V
Operating temperature:	-40 - +60 V
Service Life:	3 years
Cell type:	Primary Lithium

Condition	Discharge Current (mA)	Duration (sec)	Frequency (times per day)
BC	0,056	86296,8	1
Pulse 1	3,5	0,05	144
Pulse 2	14	0,5	144
Pulse 3	69	1	24
Pulse 4	125	1	24

Based on the information above, the following are calculated:

Condition	Discharge Current (mA)	Duration (sec)	Frequency (times per day)	C mAh per day	C mAh for 3 years
BC	0,056	86296,8	1	1,3424	1469,92216
Pulse 1	3,5	0,05	144	0,0070	7,665
Pulse 2	14	0,5	144	0,2800	306,6
Pulse 3	69	1	24	0,4600	503,7
Pulse 4	125	1	24	0,8333	912,5

Total	2,92 mAh	3 200,39 mAh

Based on these calculations and factory trials, the recommendation is a back of 4 Lithium Manganese Dioxide batteries GP CR17450 in parallel to reach a service life of 3 years. These have been performed with two primary cells GP CR123A and GP CR17450 with a discharge current of 125 mA at -40 °C to a cut-off voltage of 1.8 V.

The temperature specification for the GP CR17450 is specified to -40 to +60 °C

Looking into Lithium Thionyl batteries, they have problem delivering the needed pulse current at the lowest temperature. Adding a capacitor to the design to be able to handle the limitation, a service life of approximate 2.6 years should be possible for a single A-size Lithium Thionyl cell. The temperature range for a Lithium Thionyl cell is -55 to +85 °C.

TBD – additional simulations shall be run where temperature requirements are relaxed to -20 °C and service life lowered to 2.5 years.

SAFETY CONSIDERATIONS

Both cells that are discussed are different versions of Lithium batteries where Lithium becomes the critical point.

If it is possible to build the solution around a single cell, it becomes more simpler as there is only one cell that needs to be replaced when replacing the battery.

If several cells are needed (which is likely for some versions/use-cases), all cells need to be replaced at once. In addition, safety circuitry is needed to protect the cells. All cells need to be from a selected manufacturer.

Exemplification of problem by changing batteries:

Assume a package of two cells, should a user only replace one of two cells the fresh cell will (if not protected) try to charge the non-fresh cell. Since these are primary batteries, this is not possible, hence replacing only one cells creates a dangerous situation.

When replacing batteries, all batteries in the pack needs to be replace with batteries from the same manufacturer. Batteries from different manufacturers has different properties, hence mixing manufacturers should not be allowed.

Either special battery packs need to be designed or a disclaimer with instructions needs to be in place. The design needs to implement protective circuitry in terms of diode to prevent the cells from charring each other.

The manufacturer and model of battery becomes important since different batteries have different properties, some batteries come with internal safety functions (such as internal PTC-resistor) shutting down the battery should it become overheated. Batteries not having such function risk to be overheated.

For the suggested batteries, the Lithium Manganese Dioxide battery from GP GPCR17450 and GPCR123A has a built in temperature protection [https://www.gpbmindustry.com/product-page/gpcr17450, https://www.gpbmindustry.com/product-page/gpcr123a].

TBD – GPBM shall check if the Lithium Thionyl Batteries from Xeno is quipped with the same temperature protection.

Appendix D: INCA power subsystem evaluation [21].

E Appendices

			Digital ezPyro IR			Analog IR				
Use	Wavelength (µm)	FWHM (nm)	Single SMD	Dual SMD	2x2 SMD	TO39	Single TO39	Dual TO39	Quad TO39	Linear IR Array
Broadband for bespoke filters	2.2	LP	ePY12121	✔			PY2749			
CO_2 Optimised for max centreline sensitivity	4.35	600					PY0573			
CO_2 Optimised for uniform sensitivity across FoV	4.48	620	ePY12251	✔		ePR44252	PY1600			
CO_2 Optimised for wide FoV	4.55	420				ePR44282	PY0574			
CO_2 Optimised for wide FoV	4.64	180	ePY12241	✔					✔	
H_2O water vapour (hydrogen flame, HC flame)	2.72	200				ePR44292	PY2712			
LP Human Motion Rejection	5	LP				ePR44112	PY1601			
LP Human Motion Rejection	5.5	LP					PY0576			
Welding/sunlight rejection	3.38	190					PY1580		✔	
Welding/sunlight rejection	3.91	90	ePY12211	✔		ePR44212	PY0575		✔	

	Integrated Digital ezPyro System – single SMD	Integrated Digital ezPyro System – single TO39	Analog single TO39
Strength	• Small / low profile SMD package • Low system component count • Easy software & system development • Digital I^2C I/O	• 40% better SNR vs analog TO • Low system component count • Easy software & system development • Wide FoV / robust TO-39 package	• High sensitivity/SNR up to 20Hz • Class-leading response times • Wide FoV • Robust and compact TO-39 package
Application characteristics	• Medium range / indoor & outdoor • Small form factor • High volume deployments	• Long range / outdoor • Challenging environments • Precision detection	
Application examples	• Smart home/ building • Industrial IoT • Transportation	• Industrial • Oil & gas • Infrastructure & forest protection	• Industrial • Oil & gas • Infrastructure & forest protection
Package	SMD (5.65 x 3.70 x 1.55 mm^2)	TO-39	TO-39
Output	Digital I^2C	Digital I^2C	Analog
Integration	Configurable amplifier & filters, ADC	Configurable amplifier & filters, ADC	OpAmp
Sensitive area	0.64 x 0.64 mm^2	1.00 x 1.00 mm^2	1.00 x 1.00 mm^2
Aperture	1.65 mm ⌀	5.2 x 4.2 mm^2	5.2 x 4.2 mm^2
Time constant (10-20 Hz peak)	10 ms	10 ms	12 ms
Specific Detectivity – D* (cm√Hz/W @10Hz/500K)	2.5 x 10^8	4.8 x 10^8	3.5 x 10^8
Field of View	90 °	110 °	110 °
Range (system dependent) *demonstrated in certification environment	40 m	85 m*	65 m
Supply current	1 – 23 µA	3.5 – 23 µA	65 µA
Power saving modes	✓	✓	–
Configurability	✓	✓	–
Sensor-to-sensor synchronization	✓	–	–
Wake-up by signal	✓	–	–

Appendix E: comparison of Pyreos' Digital and Analog TO-39 pyroelectric sensor [29].

F Appendices

5/31/22, 8:51 PM Final_graphs

In [133…
```
import matplotlib.pyplot as plt
import math
import pandas
import numpy as np
import statsmodels.api as sm
```

In [134…
```
data = pandas.read_csv('Sensor_Configs.csv')
transceiver = pandas.read_csv('Transceiver.csv')
microcontroller = pandas.read_csv('Microcontroller.csv')
data.head()
```

Out[134]:

	Configuration	Sleep_Supply_Current_mA	Sampling_Supply_Current_mA	Sampling_Time_s	Idle_S
0	Sensirion SHTC3 (temperature and humidity)	0.000600	0.57000	0.0008	
1	Bosch BME680 (temperature, humidty, pressure a...	0.001000	0.09000	92.0000	
2	Sony IMX335 Camera Module (visible light)	0.000000	150.00000	15.0000	
3	Sony IMX335 Camera Module (IR)	0.000000	150.00000	15.0000	
4	T5919 (audial)	0.000009	0.00022	15.0000	

In [135…
```
#defining number of samples per hr
sampling_f = 1
#defining transciever bit rate
bit_rate = 300*8000
```

In [138…
```
x = 0
x = data.Sleep_Supply_Current_mA*((3600-(data.Sampling_Time_s+data.Power_Up_Time_s)
x = x+data.Sampling_Supply_Current_mA*(data.Sampling_Time_s*sampling_f)/3600*24
x = x+data.Idle_Supply_Current_mA*(data.Power_Up_Time_s*sampling_f)/3600*24
x = x+transceiver.Transmission_Supply_Current_mA.item()*(data.Packet_Size_bits/bit_
x = x+transceiver.Sleep_Supply_Current_mA.item()*(3600-data.Packet_Size_bits/bit_r
x = x+microcontroller.Sleep_Supply_Current_mA.item()*(3600-(data.Packet_Size_bits/
x = x+microcontroller.Active_Supply_Current_mA.item()*data.Sampling_Time_s*samplin
x = x+microcontroller.Standby_Supply_Current_mA.item()*microcontroller.Power_Up_Ti
x = 365*x
```

In [139…
```
print(type(x))
x[6] = (x.sum()-x[3])
print(x)
```

localhost:8888/nbconvert/html/Documents/Uni/ENGN2706/Power Generation IOT Project/Sensor Configurations/Final_graphs.ipynb?download=f… 1/3

Appendix F: Python code for lifetime power consumption calculations.

References

[1] World Wide Fund for Nature, "2019-20 Aus. Bushfires," [Online]. Available at: www.wwf.org.au. [Accessed: Mar. 13, 2022].

[2] N. Brew, L. Richards, and L. Smith, "2019–20 Aus. bushfires—FAQ: a quick guide," Department of Parliamentary Services, 2020. [Online]. Available: www.aph.gov.au. [Accessed: Mar. 14, 2022].

[3] Aus. Institute for Disaster Resistance, "NSW Black Summer Bushfires," n.d.. [Online]. Available: knowledge.aidr.org.au. [Accessed: Mar 14, 2022].

[4] P. Dockrill, "Fires in Australia Just Pushed Sydney's Air Quality 12 Times Above 'Hazardous' ," ScienceAlert, 2019. [Online]. Available: www.sciencealert.com. [Accessed Mar. 16, 2022].

[5] A. Dean, et al., "Summer of Crisis," Sydney: Climate Council of Australia, 2020, pp. 1-2. [Online]. Available: www.climatecouncil.org.au. [Accessed Mar. 16, 2022].

[6] J. Bishop, et al., "Fire on the Farm," The University of Sydney, 2021, p. 5. [Online]. Available: www.sydney.edu.au. [Accessed Mar. 17, 2022].

[7] Environment, Planning and Sustainable Development Directorate, "Orroral Valley Fire bushfire impact report," ACT Government, 2020. [Online]. Available: www.environment.act.gov.au. [Accessed Mar. 17, 2022].

[8] C. Allen and M. Inman, "A Defence chopper sparked Canberra's Namadgi bushfire, but its crew didn't tell authorities the location for 45 minutes," ABC News, 2020. [Online]. Available: www.abc.net.au. [Accessed Mar. 17, 2022].

[9] Qingyang, "IoT for bushfire detection," Australian National University, 2022. [Online]. Available: anu365-my.sharepoint.com. [Accessed Feb. 30, 2022].

[10] Peregian Digital Hub, "FireTech Connect," Noosa Shire Council, 2022. [Online]. Available: firetechconnect.com. [Accessed Mar. 17, 2022].

[11] Dryad, "Silvanet Wildfire Sensor Datasheet," 2020. [Online]. Available: www.dryad.net. [Accessed Mar. 25, 2022].

[12] Dryad, "Silvanet Border Gateway Datasheet," 2020. [Online]. Available: www.dryad.net. [Accessed Mar. 25, 2022].

[13] Dryad, "Silvanet Mesh Gateway Datasheet," 2020. [Online]. Available: www.dryad.net. [Accessed Mar. 25, 2022].

[14] D. Smith, "Dryad Networks launches Silvanet, aiming to save 400m tons of CO2 emissions with its ultra-early wildfire detection IoT solution," International Fire Fighter, 2021. [Online]. Available at: iffmag.mdmpublishing.com. [Accessed Mar. 25, 2022].

[15] Attentis, "Powerline Management: Keeping utilities healthy and safe.," 2022. [Online]. Available: attentistechnology.com. [Accessed Mar. 30, 2022].

[16] Attentis, "Intelligent Sensors," 2022. [Online]. Available: attentistechnology.com. [Accessed Mar. 30, 2022].

[17] Department of Infrastructure, Transport, Regional Development and Communications; "The Latrobe Valley Information Network," Aus. Gov. n.d.. [Online]. Available: www.infrastructure.gov.au. [Accessed Mar. 30, 2022].

[18] Attentis, "Latrobe Valley Information Network" 2022. [Online]. Available: lvin.org. [Accessed Mar. 30, 2022].

[19] IP Australia, "2011200992: Fire Detection," Australian Government, 2022. [Online]. Available: pericles.ipaustralia.gov.au. [Accessed Mar. 31, 2022].

[20] International Carbide Technology AB, "Technology: fire prediction," n.d.. [Online]. Available: www.incatech.se. [Accessed Apr. 17, 2022].

[21] info@incatech.se, "Research Student Enquiry," Apr. 4, 2022. [Email].

[22] NetOP Technology, "Forest Capsule," 2019. [Online]. Available: forestcapsule.netop.io. [Accessed Apr. 4, 2022].

[23] URS Forestry, "Australia's Green Triangle," Department of Agriculture, Fisheries and Forestry, n.d.. [Online]. Available: www.awe.gov.au. [Accessed Apr. 5, 2022].

[24] Green Triangle Forest Industries Hub, "About," 2022. [Online]. Available: gtfih.com.au. [Accessed Apr. 5, 2022].

[25] B. Herrmann, "South Australia's Green Triangle trials forest fire detection system as Government surveillance is reduced," ABC News, 2020. [Online]. Available: www.abc.net.au. [Accessed: Apr. 5, 2022].

[26] M. Etheridge, "South East forestry industry trials new hi-tech equipment, software to keep an eye on fire hot spots," The Advertiser, 2020. [Online]. Available:

www.workingonfire.com.au. [Accessed: Apr. 5, 2022].

[27] Tasmanian Forests and Forest Products Network, "Trial of early forest fire detection technology decreases response times and increases safety," 2021. [Online]. Available: www.tffpn.com.au. [Accessed: Apr. 5, 2022].

[28] Pyreos, "Case studies," n.d.. [Online]. Available: https://pyreos.com/case-studies/. [Accessed: Apr. 12, 2022].

[29] Pyreos, "Flame detection," n.d.. [Online]. Available: pyreos.com. [Accessed: Apr. 12, 2022].

[30] Pyreos, "TETHIR AND PYREOS CONSORTIUM WINS £0.5M UK GRANT FOR IOT SENSOR NETWORKS FOR FASTER FOREST FIRE DETECTION," 2021. [Online]. Available: pyreos.com. [Accessed: Apr. 12, 2022].

[31] Parallel Flight Technologies, "Firefly Heavy-Life UAS," n.d.. [Online]. Available: parallelflight.com. [Accessed: Apr. 6, 2022].

[32] U. Dampage, et al., "Forest fire detection system using wireless sensor networks and machine learning," Nature, 2022. [Online]. Available: www.nature.com. [Accessed Mar. 15, 2022].

[33] P. Rilko "Wireless Sensing for Bushfire Detection through Sound Spectrum Analysis," Australian National University, 2021. [Online]. Available: anu365-my.sharepoint.com. [Accessed Feb. 30, 2022].

[34] H. Kaur, "Bushfire Detection using Vision Based Systems," Australian National University, 2021. [Online]. Available: anu365-my.sharepoint.com. [Accessed Feb. 30, 2022].

[35] D. Lee, et al., "Energy harvesting using thermoelectricity for IoT (Internet of Things) and E-skin sensors," J. of Phys. Energy, 2019. [Online]. Available: www.researchgate.net. [Accessed Apr. 29, 2022].

[36] A. Agbossou, et al., "On thermoelectric and pyroelectric energy harvesting," Smart Materials and Structures, 2009. [Online] Available: www.researchgate.net. [Accessed Apr. 29, 2022].

[37] A. Kumar, et al., "Pyroelectric Energy Conversion and Its Applications—Flexible Energy Harvesters and Sensors," Sensors MPDI, 2019. [Online]. Available: www.ncbi.nlm.nih.gov. [Accessed Apr. 29, 2022].

[38] H.K. Cha, et al., "RF power harvesting: a review on designing methodologies and applications," Micro and Nano Systems Letters, 2017. [Online]. Available: mnsl-journal.springeropen.com. [Accessed Apr. 29, 2022].

[39] Z. Han, et al., "Wireless Networks With RF Energy Harvesting: A Contemporary Survey," IEEE, 2014. [Online]. Available: ieeexplore.ieee.org. [Accessed Apr. 29, 2022].

[40] Australian Communications and Media Authority, "Spectrum Licenses," Aus. Gov., 2021. [Online]. Available: acma.gov.au. [Acessed May 15, 2022].

[41] Forbes, "Semtech (SMTC)," 2022. [Online]. Available: forbes.com. [Accessed May 17, 2022].

[42] Semtech, "LoRa Technology: Overview," 2022. [Online]. Available: semtech.com. [Accessed May 17, 2022].

[43] LoRa Developer Portal, "LoRa Developer Guide," Semtech, 2022. [Online]. Available: semtech.com. [Accessed May 17, 2022].

[44] Behrtech, "Example mesh network topology," 2018. [Image]. Available: behrtechnologies.com. [Accessed 30 May, 2022].

[45] L Casals, et al., "Modelling the energy performance of LoRaWAN," Sensors MPDI, 2017. [Online]. Available: researchgate.net. [Accessed May 4, 2022].

[46] ST Microelectronics, "STM32L496xx Datasheet," 2022. [Online]. Available: st.com. [Accessed 17 May, 2022].

[47] ST Microelectronics, "STM32L496xx Sample and Buy," 2022. [Online]. Available. st.com. [Accessed 17 May, 2022].

[48] A. Sullivan, "Bushfires in Australia: Understanding Hell on Earth," CSIRO, 2022. [Online]. Available: ecos.csiro.au. [Accessed 3 May, 2022].

[49] A. Jain, "Types of Temperature Sensor," GeeksforGeeks, 2021. [Online]. Available: geeksforgeeks.org. [Accessed 17 May, 2022].

[50] D. Lloyd, et al, "Thermocouples," Encyclopedia of Medical Devices and Instrumentation, 2006. pp.340-342 [Online]. Available: researchgate.net. [Accessed 17 May, 2022].

[51] AMS, "AS621x Datasheet," 2022. [Online]. Available: ams.com. [Accessed 17 May, 2022].

[52] Sensirion. "STS4x Datasheet," 2022. [Online]. Available: sensirion.com. [Accessed 17 May, 2022].

[53] Bosch Sensortec. "BME680 Datasheet," 2022. [Online]. Available: bosch-sensortec.com. [Accessed 17 May, 2022].

[54] N. Varela, et al, "Wireless sensor network for forest fire detection," 15th International Conference on Future Networks and Communications, 2020. [Online]. Available: sciencedirect.com. [Accessed 12 May, 2022]

[55] Switches International, "Types of Humidity Sensors," 2021. [Online]. Available: switches.co.za. [Accessed 12 May, 2022].

[56] Sensirion, "SHTC3 Datasheet," 2021. [Online]. Available: sensirion.com. [Accessed 15 May, 2022].

[57] Mouser, "DHT11 Datasheet," n.d.. [Online]. Available: mouser.com. [Accessed 15 May, 2022].

[58] Sensirion, "SHT3x Datasheet," 2021. [Online]. Available: sensirion.com. [Accessed 15 May, 2022].

[59] Science Learning Hub NZ, "What is smoke?" 2009. [Online]. Available: science-learn.org.nz. [Accessed 8 May, 2022].

[60] GDS Corp, "VOC sensors: working principles," 2020. [Online]. Available: gdscorp.com. [Accessed 8 May, 2022].

[61] Sensirion, "SGP40 Datasheet," 2022. [Online]. Availale: sensirion.com. [Accessed 8 May, 2022].

[62] National Institute of Standards and Technology, "How do smoke detectors work?" 2022. US Gov. [Online]. Available: nist.gov. [Accessed 8 May, 2022].

[63] VIEWSPACE, "Seeing through smoke," n.d.. [Online]. Available: viewspace.org. [Accessed 1 May, 2022].

[64] RP Photonics, "Pyroelectric detectors," n.d.. [Online]. Available: rp-photonics.com. [Accessed 1 May, 2022].

[65] School of Physics, "Pyroelectric effect," n.d.. University of Melbourne. [Online] Available: ph.unimelb.edu.au. [Accessed 1 May, 2022].

[66] AZO Sensors, "Hydrocarbon fire typical emission spectrum," 2017. [Image]. Available: azosensors.com. [Accessed 1 May, 2022].

[67] Camera-module.com, "Sony IMX335 5MPx Visible Light Camera Module," 2022. [Online]. Available: camera-module.com. [Accessed 27 Apr, 2022].

[68] oemcameramodules.com, "Sony IMX335 5MPx Infrared Camera Module," 2022. [Online]. Available: oemcameramodules.com. [Accessed 27 Apr, 2022].

[69] Mouser, "T5919 Datasheet," 2022. [Online]. Available: au.mouser.com. [Accessed 30 Apr. 2022].

[70] M. Olson, "Redox reactions," 2021. Encyclopedia Britannica. [Online]. britannica.com. [Accessed 25 May, 2022].

[71] S. Farahani, "Zigebee Wireless Networks and Transceivers," 2008. Chapter 6. pp. 207-211. [Online] Available: books.google.com.au [Accessed 21 May, 2022].

[72] M.K. Hill, "Understanding Environmental Pollution," 2004. Cambridge University Press. [Online]. Available: archieve.org. [Accessed 25 May, 2022].

[73] M.B. Tahir, "Nanotechnology: the road ahead," 2020. University of Gujrat. pp. 296-299 [Online]. Available: sci-hub.se. [Accessed 25 May, 2022].

[74] J. Geisz, et al., "Six-junction III–V solar cells with 47.1% conversion efficiency under 143 Suns concentration," 2020. Nature. [Online]. Available: nature.com. [Accessed 25 May, 2022].

[75] NREL. "Best research cell efficiencies," 2022. [Image]. Available: nrel.gov. [Accessed 25 May, 2022].

[76] P. Ribeyron, "Crystalline silicon solar cells: better than ever," 2017. Nature. [Online]. Available: nature.com. [Accessed 25 May, 2022].

[77] V. Dutta, et al., "Thin film solar cells: an overview," 2004. Academia. [Online]. Available: academia.edu. [Acessed 27 May, 2022].

[78] toolstud.io, "Video and audio file size calculator," 2022. [Online]. Available: toolstud.io. [Accessed 30 May, 2022].